NATIONAL ADVISORY COMMITTEE FOR AERONAUTICS

WARTIME REPORT

ORIGINALLY ISSUED
September 1943 as
Advance Confidential Report 3I14

WIND-TUNNEL TESTS OF AILERONS AT VARIOUS SPEEDS

III - AILERONS OF 0.20 AIRFOIL CHORD AND TRUE CONTOUR WITH 0.35-AILERON-CHORD FRISE BALANCE ON THE NACA 23012 AIRFOIL

By W. Letko and W. B. Kemp

Langley Memorial Aeronautical Laboratory
Langley Field, Va.

WASHINGTON

NATIONAL ADVISORY COMMITTEE FOR AERONAUTICS

ADVANCE CONFIDENTIAL REPORT

WIND-TUNNEL TESTS OF AILERONS AT VARIOUS SPEEDS

III - AILERONS OF 0.20 AIRFOIL CHORD AND TRUE CONTOUR WITH 0.35-AILERON-CHORD FRISE BALANCE ON THE NACA 23012 AIRFOIL

SUMMARY

Hinge moment, lift, and pressure-distribution measurements were made on a Frise aileron on an NACA 23012 airfoil in the two-dimensional test section of the LMAL stability tunnel. Speeds up to 360 miles per hour corresponding to a Mach number of about 0.470 were used. The nose radius of the aileron was varied from 0.0012 to 0.0150 of the airfoil chord. Tests also were made with an increased vent gap and with the lower surface of the airfoil at the entrance of the slot rounded to a radius of 0.02 of the airfoil chord. The primary purpose of all tests was to determine the effects of speed on this type of aileron.

The variation in section hinge-moment and section lift coefficient with Mach number and angle of attack is shown in curves of hinge-moment and lift coefficient plotted against aileron deflection for the various conditions tested. Slopes of these curves were determined and plotted against Mach number and aileron nose radius.

Increases in speed decreased the unstalled range of negative aileron deflections. The changes in hinge-moment coefficients with speed seem comparatively small in the unstalled range but would probably cause considerable error if neglected in computing the stick forces for high speeds.

For small aileron deflections the aileron with the smallest nose radius was most effective in reducing hinge moments, but the negative range of balance effectiveness was very limited. Increasing the nose radius extended the negative range of balance effectiveness appreciably, increased the negative range in which the aileron was

effective in producing increments of lift, and caused a considerable increase in the lift produced by the aileron at high angles of attack and large positive aileron deflections. Rounding the lower surface of the airfoil at the slot entrance and increasing the vent gap had an appreciable but varying effect on the lift and hinge-moment coefficients, depending on the angle of attack and aileron deflection.

Oscillations of the Frise ailerons occurred at the negative angle of stall of the ailerons. A vibration of shudder different from the usual oscillation occurred at the high speeds at large angles of attack and at small and even zero aileron deflections.

INTRODUCTION

Increases in the size and speed of combat airplanes, together with the demand for high rolling velocities, have made it necessary to balance almost completely the hinge moments of control surfaces in order to enable the pilot to deflect the controls under all conditions of flight. Because this close balance and the compressibility effects have caused overbalance with some existing aileron installations at high airspeeds, some of the currently used or recently proposed balance arrangements must be retested.

The NACA is undertaking a study of some of the more promising aileron forms at airspeeds higher than those employed in previous developments. Results of tests of a blunt-nose and a sealed-internal-balance aileron on a low-drag airfoil section are reported in references 1 and 2. The section characteristics of a Frise aileron of 0.20 airfoil chord and 0.35-aileron-chord balance on an NACA 23012 airfoil are presented herein.

The section lift and section hinge-moment coefficients were measured at different airspeeds up to speeds of 360 miles per hour (Mach number of 0.470) through an angle of attack range of -5° to 10° and an aileron deflection range of $\pm 20^\circ$. The influence of the aileron nose radius and the effect of rounding the lower airfoil surface at the entrance of the slot and of increasing the vent gap were also investigated. The results are presented as curves of section lift coefficient and section hinge-moment coefficient plotted against aileron deflection. The slopes of

the curves were plotted against Mach number and aileron nose radius to show the effect of changes in the shape of the aileron balance.

SYMBOLS

The coefficients and symbols used in this paper are defined as follows:

c_l airfoil section lift coefficient $\left(\frac{l}{qc}\right)$

c_{h_a} aileron section hinge-moment coefficient $\left(\frac{h_a}{qc_a^2}\right)$

where

l airfoil section lift

h_a aileron section hinge moment

c chord of basic airfoil, including aileron

c_a chord of the aileron measured from the hinge axis back to the trailing edge

q dynamic pressure $\left(\frac{1}{2}\rho V^2\right)$

V absolute air velocity

ρ mass density of air

and

R aileron nose radius, fraction of chord

α_o angle of attack for airfoil of infinite aspect ratio

δ_a aileron angle with respect to airfoil, considered positive with trailing edge down

M Mach number

$\left(\frac{\partial c_{h_a}}{\partial \delta_a}\right)_{\alpha_o}$ slope of c_{h_a} against δ_a at constant α_o

$\left(\frac{\partial c_l}{\partial \delta_a}\right)_{\alpha_o}$ slope of c_l against δ_a at constant α_o

$\left(\frac{\partial c_l}{\partial \alpha_o}\right)_{\delta_a = 0}$ slope of c_l against α_o at $\delta_a = 0$

APPARATUS AND MODELS

The tests were made in the NACA two-dimensional test section of the stability tunnel. This section is rectangular, 6 feet high and 2.5 feet wide. Speeds up to 360 miles per hour corresponding to a Mach number of 0.470 were used. Figure 1 shows the model mounted in the tunnel.

The model of 2-foot chord and 2.5-foot span had an NACA 230.2 airfoil section. The main portion of the airfoil model was made of laminated mahogany. The 0.20c Frise aileron with $0.35c_a$ balance was made of steel with wooden nose pieces. Figure 2 is a sketch showing the dimensions and configurations of the aileron tested.

The aileron was supported at the ends by ball bearings fitted into steel end plates that were attached to the main airfoil. The airfoil which completely spanned the tunnel was fixed into circular end plates that were set flush with the tunnel wall.

The angle of attack of the model was changed by rotating the end plates. The aileron deflection and the hinge moments were measured by a calibrated spring-torque-and-sector system. In some cases the hinge moments were also obtained from the pressure distribution over the aileron. The lift was measured by an integrating manometer connected to orifices in the tunnel floor and ceiling and was calibrated against lift obtained by pressure distribution. Pressure orifices, which were located along the midspan of the wing and aileron, were connected to a

multiple-tube manometer, and the pressures were recorded photographically.

TESTS

Tests were made on an NACA 23012 airfoil equipped with a Frise aileron for aileron nose radii of 0.0012c, 0.008c, and 0.0150c with a constant nose gap of 0.005c and a constant vent gap of 0.0055c. The lower surface of the airfoil at the slot entrance was not rounded for these tests. (See fig. 2.) With the lower surface at the slot entrance rounded to a 0.02c radius, additional tests were made for the aileron with nose radius of 0.008c and a nose gap of 0.005c but with the vent gap equal to 0.0055c and 0.01c.

Section hinge moments and section lift were measured for speeds from 150 to 360 miles per hour corresponding to Mach numbers ranging from 0.195 to 0.470. The lowest speed corresponded to a Reynolds number of about 2,800,000 and the highest speed to a Reynolds number of about 6,700,000. The relation between Reynolds number for standard atmospheric conditions and test Mach number is shown in figure 3.

The tests were made at angles of attack of -5°, 0°, 5°, and 10° and for each angle of attack readings were taken at aileron deflections of 0°, $\pm 2^\circ$, $\pm 5^\circ$, $\pm 7^\circ$, $\pm 10^\circ$, $\pm 13^\circ$, $\pm 15^\circ$, $\pm 18^\circ$, and $\pm 20^\circ$.

Pressure-distribution records were obtained at Mach numbers of 0.199, 0.358, and 0.470 for every angle of attack tested. For each angle of attack records were made at aileron deflections of 0°, $\pm 5^\circ$, $\pm 10^\circ$, and $\pm 15^\circ$.

PRECISION

Angles of attack were set to within $\pm 0.1^\circ$ and aileron deflections to within $\pm 0.3^\circ$. Measurements of the hinge-moment coefficients could be repeated to within ± 0.003 and lift coefficients to within ± 0.01.

Corrections for tunnel-wall effects were not applied to the hinge-moment coefficients. The aileron angles were corrected for torsional deflection under load. The following corrections were applied to the section lift coefficients and the angle of attack:

$$c_l = \left[1 - Y\,(1 + 2\beta)\right] c_l'$$

$$\alpha_o = (1 + Y)\,\alpha_o'$$

where

$$Y = \frac{\pi^2}{48}\left(\frac{c}{h}\right)^2$$

$\beta = 0.237$ (a theoretical factor for NACA 23012 airfoil)

h height of tunnel

c_l' measured lift coefficient

α_o' uncorrected or geometric angle of attack

The values used are:

$$c_l = 0.966\, c_l'$$

$$\alpha_o = 1.023\, \alpha_o'$$

Hinge moments were measured both by pressure distribution and by the spring torque balance for a number of conditions and the results are plotted in figure 4. The variations shown are probably attributable to the fact that the spring balance measures the moment on the entire aileron, which includes the effects of tunnel-wall boundary layer and of gaps at the ends of the aileron as well as any cross flow over the aileron. The pressure distribution, however, gives the hinge moment at the midsection of the aileron and is subject to errors in fairing the pressure-distribution diagrams.

RESULTS AND DISCUSSION

For most of the speed and angle-of-attack ranges, only small changes were observed in the general behavior

of the Frise ailerons. At the negative angle of stall of the aileron, which depended on the angle of attack, the speed, and the shape of the aileron balance, the aileron would oscillate between the stalled and the unstalled condition.

A different effect was noted at an angle of attack of 10°, where at high speeds a violent, intermittent vibration or shudder occurred at small positive aileron deflections. Simultaneously, an intermittent stall of the whole upper surface occurred as was shown by the tufts which were placed over the wing and aileron in order to study this phenomenon. With further increases of speed this effect took place at still lower positive, and even at small negative, aileron deflections and at lower angles of attack.

The violent vibration or shudder may have been the result of compressibility shock over the wing and aileron because, in all cases in which the vibration occurred, the peak pressures on the upper surface of the wing were found to be uniformly higher than the critical pressure. It is also probable that the vibration may be associated with some peculiarity in the model mounting, irregularities in aileron profile, or static unbalance of the aileron. Changes in the shape of the slot and sealing the slot with plasticine had no apparent effect on the vibration. When a blunt-nose aileron was tested under the same conditions on the same wing, however, the vibration did not occur.

The possibility of damage to the model and equipment because of the violence and spasmodic occurrence of the vibration limited the investigation of this phenomenon with the result that neither the cause nor the effect was definitely determined. The widespread use of the Frise aileron, however, warrants a further investigation of this vibration.

Hinge Moments

The aileron section hinge-moment coefficients c_{h_a} plotted against aileron deflection δ_a for the various speeds and aileron parameters are given in figures 5 to 9. These curves show that for positive aileron deflections the slopes of the curves of c_{h_a} against δ_a

become more negative with increasing δ_a; whereas for negative aileron deflections, the slopes of the curves are generally small and sometimes become slightly positive for a limited range of δ_a. After the aileron stalls, the slopes suddenly increase with the result that the magnitude of the hinge moment at large negative deflections is about the same as that at corresponding positive deflections.

Even though the results show that the individual aileron was usually overbalanced for some negative deflections, the combination of two ailerons on an airplane would not necessarily be overbalanced. Certain linkage combinations, however, might give overbalance.

The range of negative aileron deflections, for which good balance of hinge moments is obtained, decreases with increased speed and increases with increased aileron nose radius, as is shown in figures 5, 6, and 7. The amount of unbalance increases with increased α_o for positive aileron deflections and decreases with increased α_o for negative aileron deflections, except when $\alpha_o = -5^\circ$, at which the hinge moments are much larger than when $\alpha_o = 10^\circ$.

Because the effects, in the unstalled range, of the various aileron and test parameters are not readily apparent from the curves of figures 5 to 9, the values of $\left(\frac{\partial c_{h_a}}{\partial \delta_a}\right)_{\alpha_o}$ obtained from the values of c_{h_a} at $\pm 5^\circ$ aileron deflection are plotted against M in figures 10(a) and 10(b). These figures show an appreciable change in $\left(\frac{\partial c_{h_a}}{\partial \delta_a}\right)_{\alpha_o}$ with increases in speed. The direction and magnitude of the change depends on the angle of attack and the aileron parameters. Figure 10(b) shows that when the lower surface was rounded to a 0.02c radius the absolute value of $\left(\frac{\partial c_{h_a}}{\partial \delta_a}\right)_{\alpha_o}$ increased at positive angles of attack

and decreased at negative angles of attack. Increasing the vent gap generally decreased the absolute value of $\left(\frac{\partial c_{h_a}}{\partial \delta_a}\right)_{\alpha_o}$.

The effect of aileron nose radius on $\left(\frac{\partial c_{h_a}}{\partial \delta_a}\right)_{\alpha_o}$ is shown in figure 11. The value of $\left(\frac{\partial c_{h_a}}{\partial \delta_a}\right)_{\alpha_o}$ increased negatively with aileron nose radius and the largest changes occurred at the high angles of attack.

The value of $\left(\frac{\partial c_{h_a}}{\partial \delta_a}\right)_{\alpha_o}$ obtained for the ailerons with a nose radius of 0.0150c probably could be decreased to approximately the value obtained for the ailerons with a nose radius of 0.0012c by use of a small amount of additional balance; at the same time, the negative range of balance effectiveness would be larger than the negative range obtained with the small nose radius.

Lift

The airfoil section lift coefficients c_l obtained with the integrating manometer for zero aileron angle, are presented as a function of α_o in figures 12(a) and 12(b) for the various speeds and aileron parameters tested. The results indicate that generally, at an angle of attack of 10°, the value of c_l is higher than the value usually obtained for a plain 23012 airfoil. This increase is probably due to the effect of the slot because c_l increased when the nose radius increased and when the lower surface of the airfoil was rounded at the entrance of the slot.

As was expected, increasing the speed increased the slope of the lift curve. This effect is shown in figure 13, which is a plot of lift-curve slope obtained from values of c_l at $\alpha_o = \pm 5°$, against Mach number for the different aileron parameters. For comparison, a curve

is included with values of $\left(\frac{\partial c_l}{\partial \alpha_o}\right)_{\delta_a}$ that are increased by the factor $\frac{1}{\sqrt{1 - M^2}}$, which is the theoretical variation of lift-curve slope with M as given in reference 3.

The variation of section lift coefficient c_l with aileron angle is given in figures 14 to 18; in order to avoid confusion, only the curves for the medium speed were faired. The values of c_l are approximately proportional to aileron deflections extending to about 20° in the positive direction. The aileron stall, which depends on nose radius and α_o for a given speed, occurs at a much lower negative aileron deflection, however, and the increment of c_l due to aileron deflection decreases for greater values of δ_a. The range of negative aileron deflections in which the aileron is not stalled decreases with increases of speed and increases with increases in nose radius.

The slopes of the curves are generally lowest at $\alpha_o = 0°$ and, in most cases, the slope increases as α_o changes in eigher direction. The effect of speed on $\left(\frac{\partial c_l}{\partial \delta_a}\right)_{\alpha_o}$ is best shown by figures 19(a) and 19(b), which give the curves of $\left(\frac{\partial c_l}{\partial \delta_a}\right)_{\alpha_o}$ plotted against M for all aileron parameters. The values of $\left(\frac{\partial c_l}{\partial \delta_a}\right)_{\alpha_o}$ were obtained from the values of c_l at $\delta_a = \pm 5°$. The slopes increase with Mach number in a manner similar to the increase in the slopes of the curves of c_l against α_o given in figure 13.

Changing the aileron nose radius had an appreciable effect on $\left(\frac{\partial c_l}{\partial \delta_a}\right)_{\alpha_o}$ as shown in figure 20. At low and

negative angles of attack $\left(\frac{\partial c_l}{\partial \delta_a}\right)_{\alpha_o}$ generally decreased as the nose radius increased but at high angles of attack increased with increased nose radius. The absolute value of $\left(\frac{\partial c_l}{\partial \delta_a}\right)_{\alpha_o}$ generally decreased at low and negative angles of attack but was increased at medium and high angles of attack as a result of rounding the lower surface of the airfoil at the slot entrance. (See fig. 20.) An increase in the vent gap caused a decrease in $\left(\frac{\partial c_l}{\partial \delta_a}\right)_{\alpha_o}$ for all angles of attack, the effect being much larger at low and medium angles of attack than at high angles of attack (fig. 20).

CONCLUSIONS

The results of the tests of Frise ailerons of 0.20 airfoil chord and true contour with 0.35 aileron-chord balance on the NACA 23012 airfoil indicate the following general conclusions:

1. The unstalled range of negative aileron deflections was decreased by increasing the airspeed; in the unstalled range, however, the changes in hinge-moment coefficients with speed were comparatively small and irregular for the speed range tested but would probably cause a considerable error if neglected in computing stick forces for high speeds.

2. For small aileron deflections the aileron with the smallest nose radius tested was most effective in reducing hinge moments, but the effective range was limited. Increasing the nose radius produced a large increase in the range of negative aileron angles at which the aileron was effective in producing increments of lift. Increases in nose radius also caused a considerable increase in the lift produced by the aileron at high angles of attack and large positive aileron deflections.

3. Rounding the lower surface of the airfoil at the slot entrance and increasing the vent gap had an appreciable but irregular effect on the lift and hinge-moment coefficients, depending on angle of attack and aileron deflection.

4. Oscillations of the Frise ailerons occurred at the negative angle of stall of the ailerons. A vibration or shudder different from the oscillation occurred at the high speeds at large angles of attack and at small and even zero aileron deflections.

Langley Memorial Aeronautical Laboratory,
National Advisory Committee for Aeronautics,
Langley Field, Va.

REFERENCES

1. Letko, W., Denaci, H. G., and Freed, C.: Wind-Tunnel Tests of Ailerons at Various Speeds. I - Ailerons of 0.20 Airfoil Chord and True Contour with 0.35 Aileron-Chord Extreme Blunt Nose Balance on the NACA 66,2-216 Airfoil. NACA ACR No. 3F11, 1943.

2. Denaci, H.G., and Bird, J. D.: Wind-Tunnel Tests of Ailerons at Various Speeds. II - Ailerons of 0.20 Airfoil Chord and True Contour with 0.60 Aileron-Chord Sealed Internal Balance on the NACA 66,2-216 Airfoil. NACA ACR No. 3F18, 1943.

3. Glauert, H.: The Effect of Compressibility on the Lift of an Aerofoil. R. & M. No. 1135, British A.R.C., 1928.

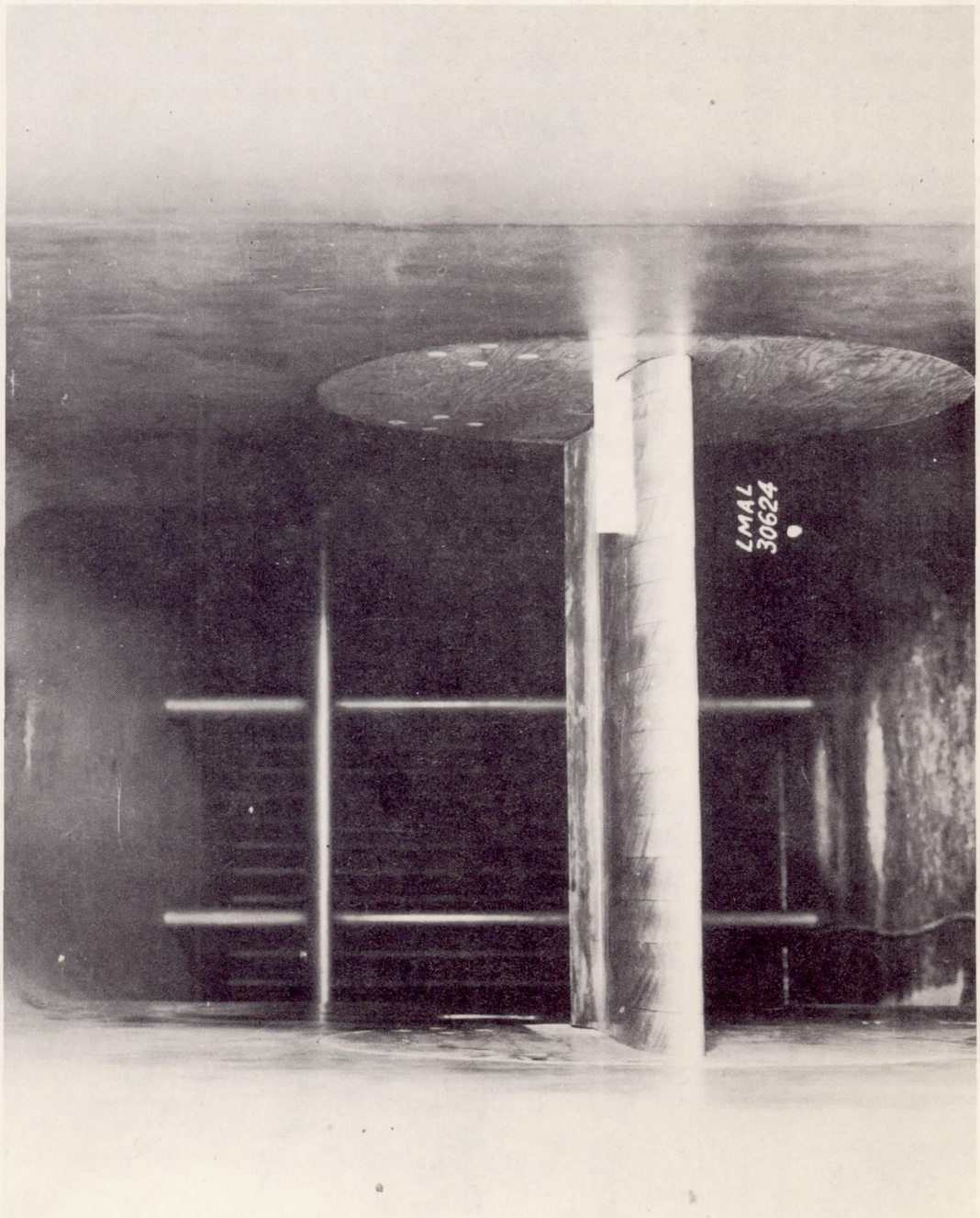

Figure 1.- Airfoil and aileron mounted in tunnel.

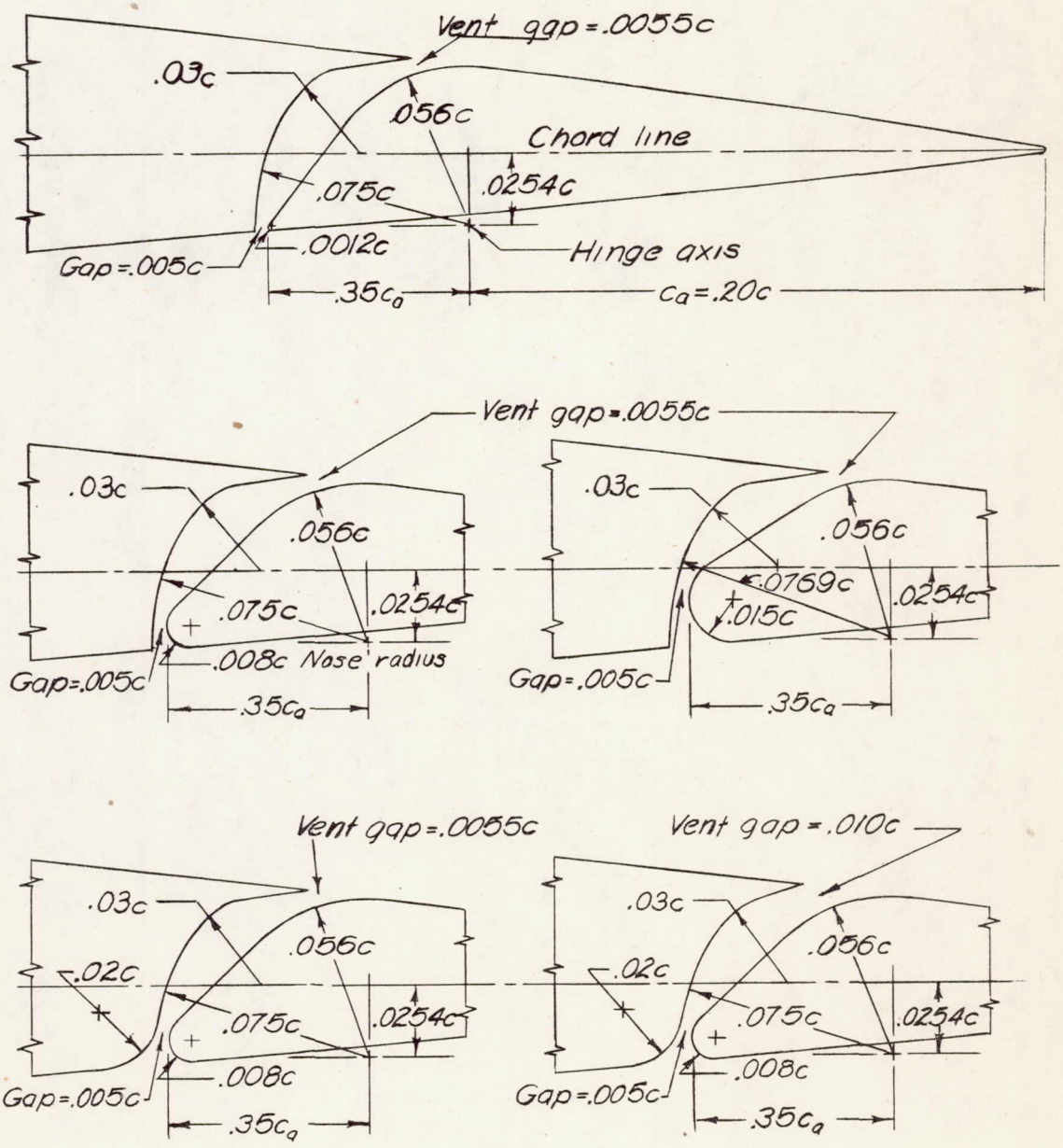

Figure 2.- Dimensions of Frise ailerons.

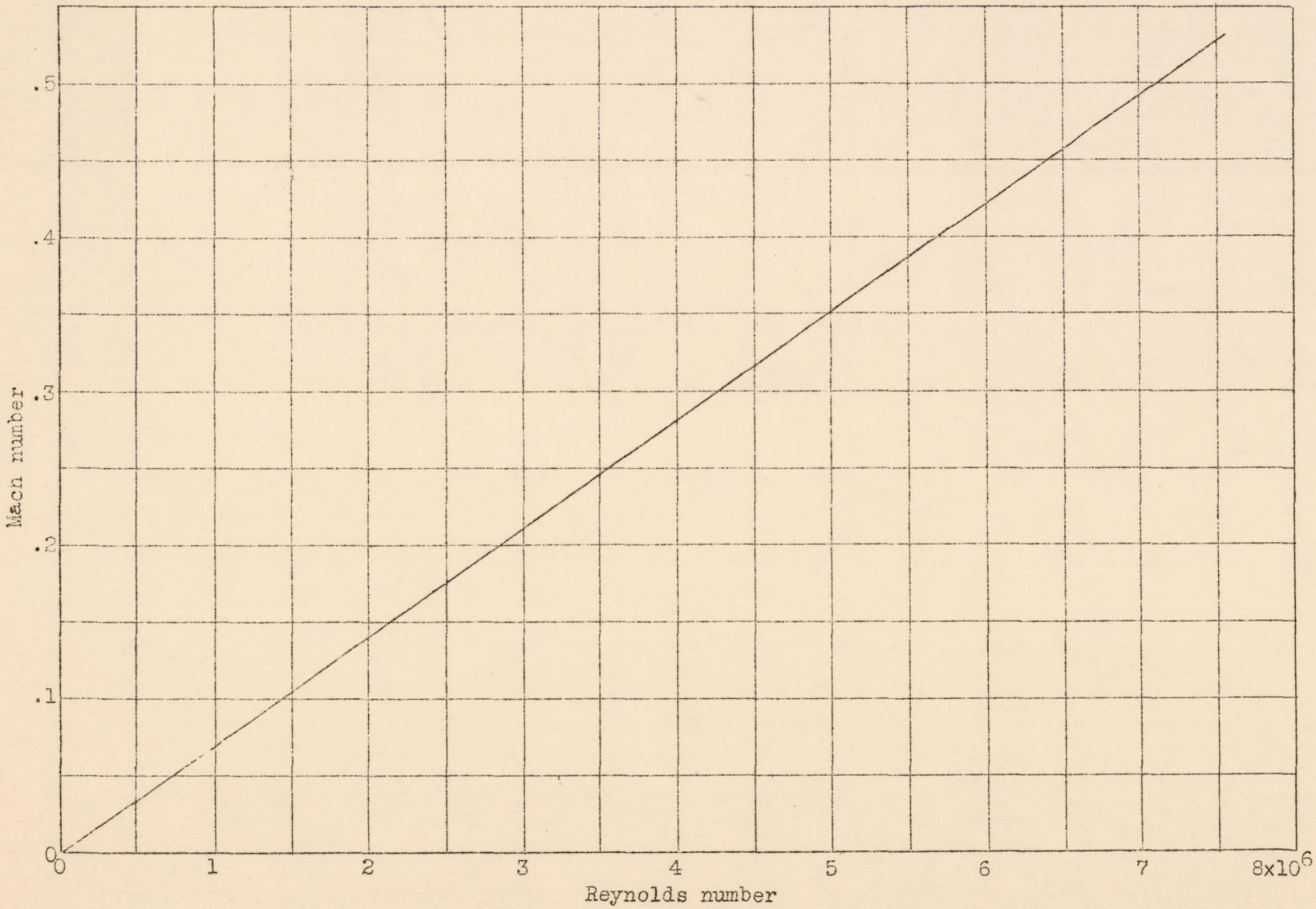

Figure 3.- Variation of test Mach number with Reynolds number, based on standard atmosphere, for a 2-foot chord airfoil in the 2.5-by 6-foot test section of the stability tunnel.

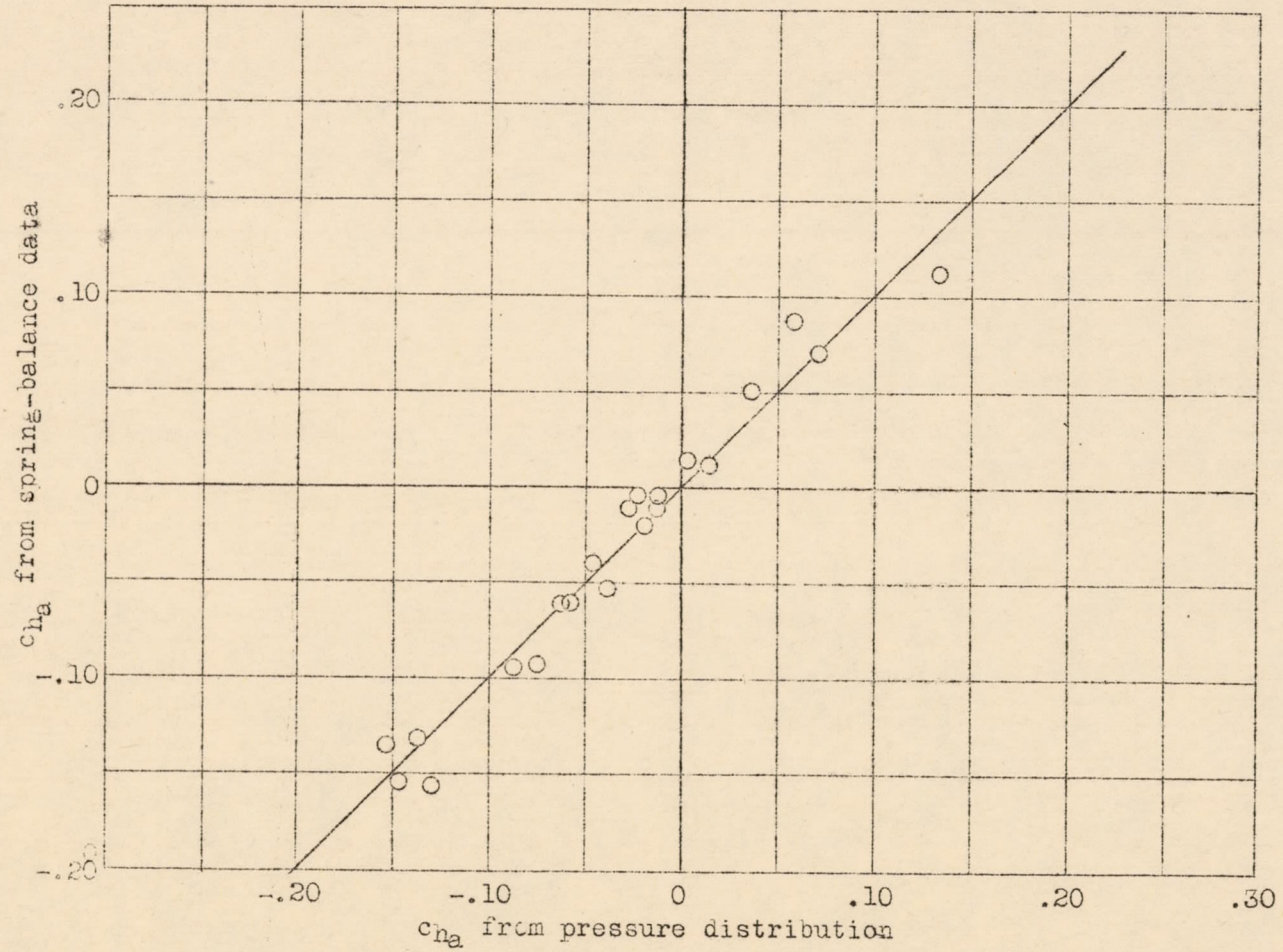

Figure 4.- Comparison of hinge-moment coefficients obtained from spring-balance data with those obtained from pressure distribution.

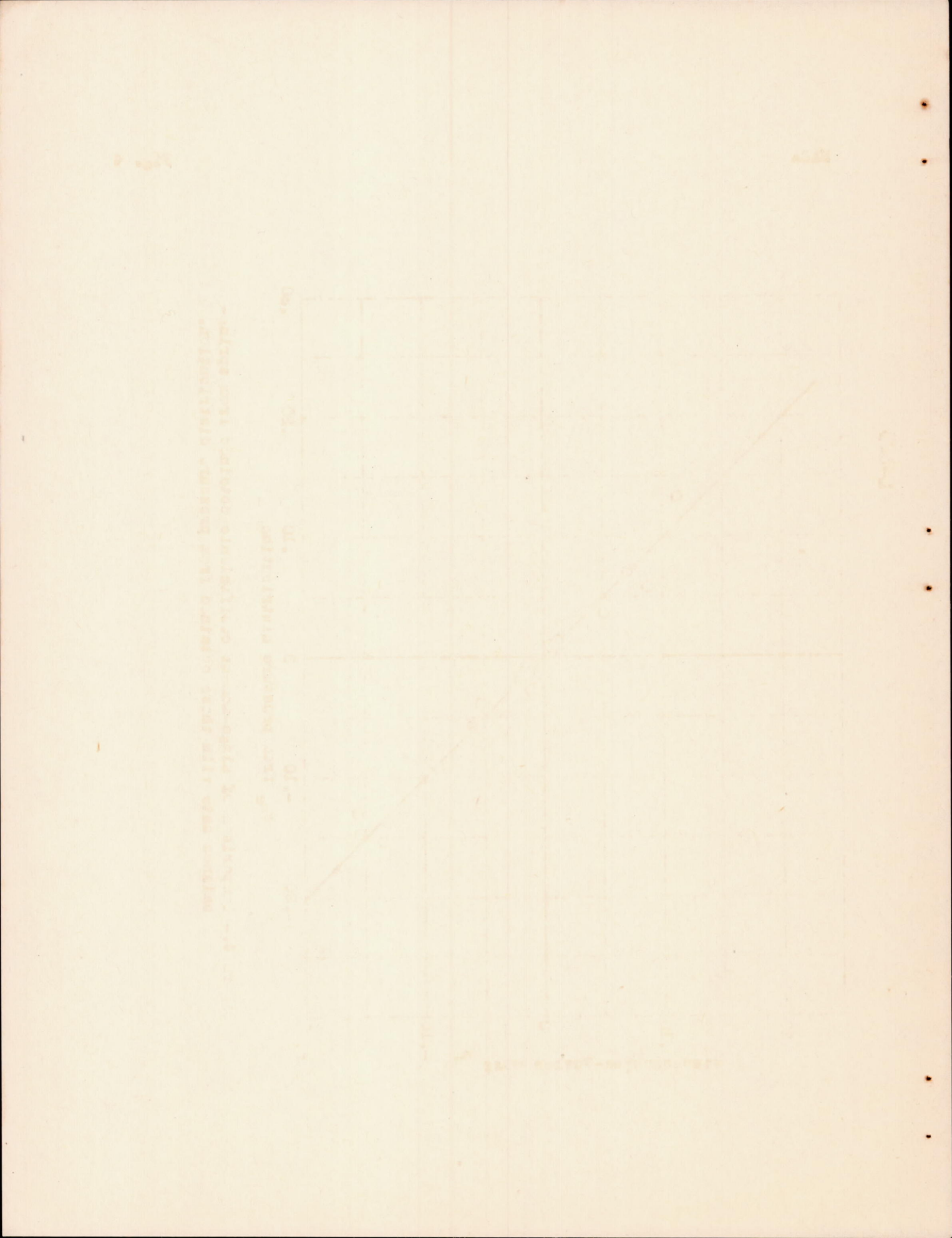

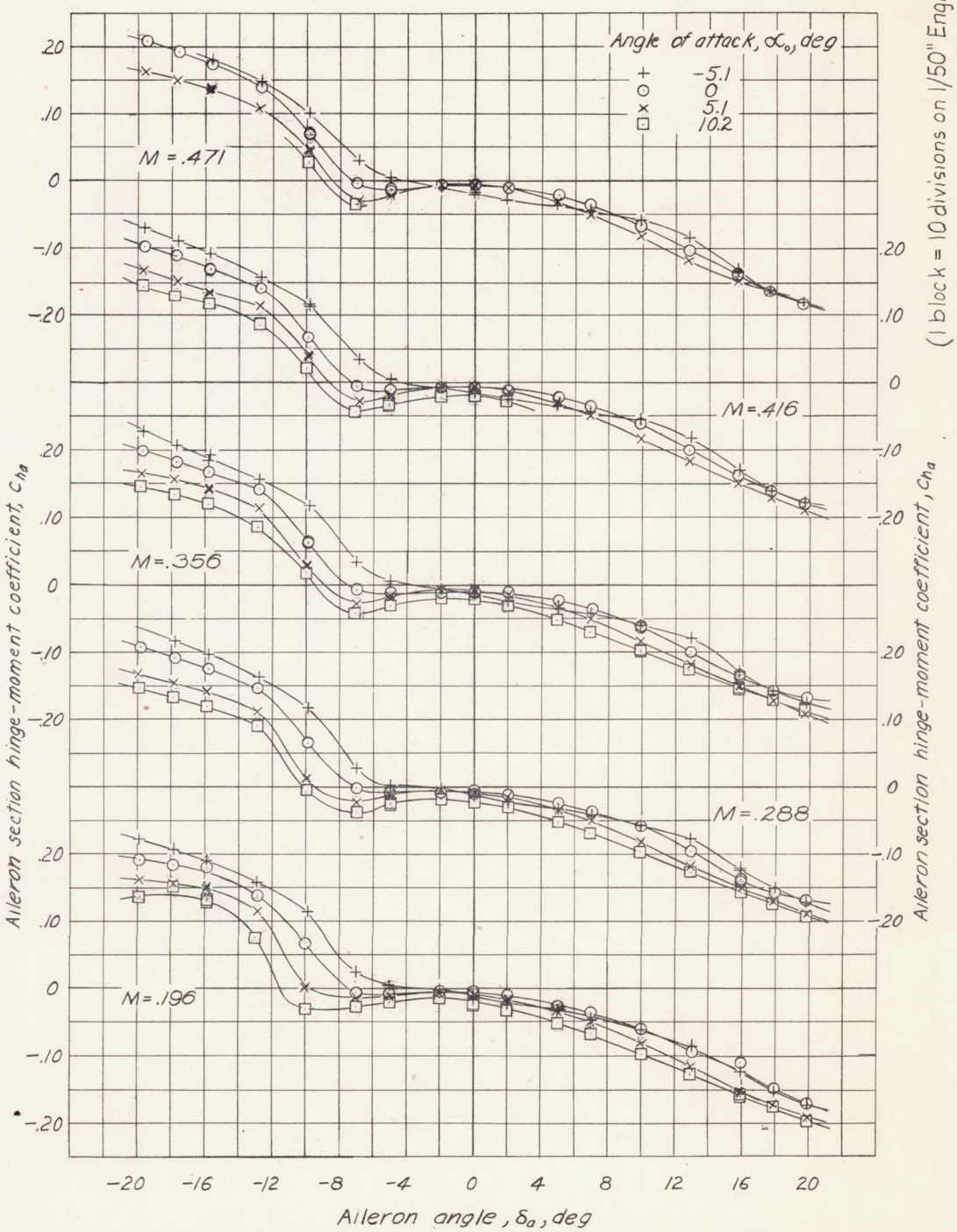

Figure 5.— Variation of aileron section hinge-moment coefficient with aileron angle. Aileron-nose radius=0.0012c; lower-surface radius=0; vent gap=0.0055c.

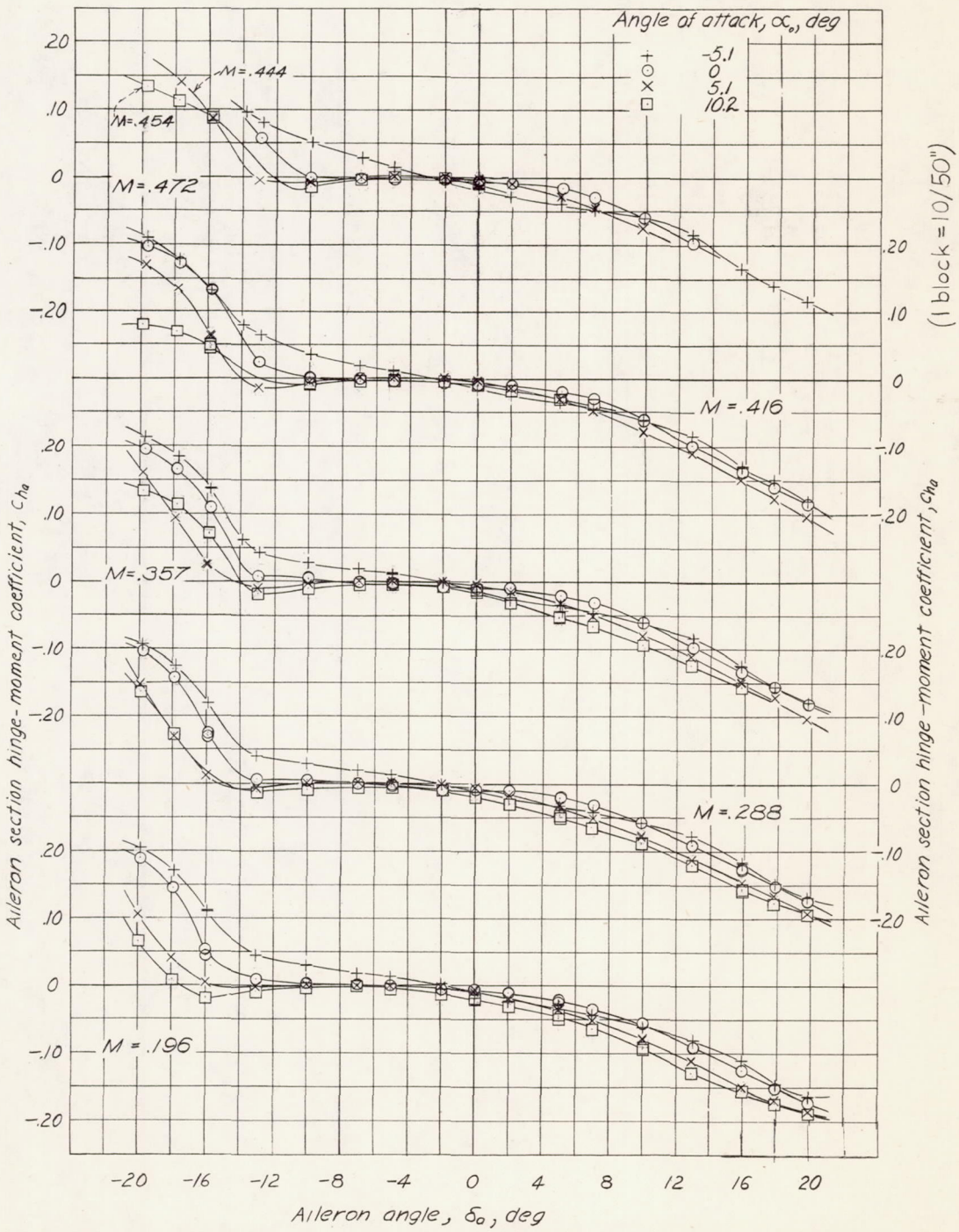

Figure 6. – Variation of aileron section hinge-moment coefficient with aileron angle. Aileron-nose radius=0.008c; lower-surface radius=0; vent gap=0.0055c.

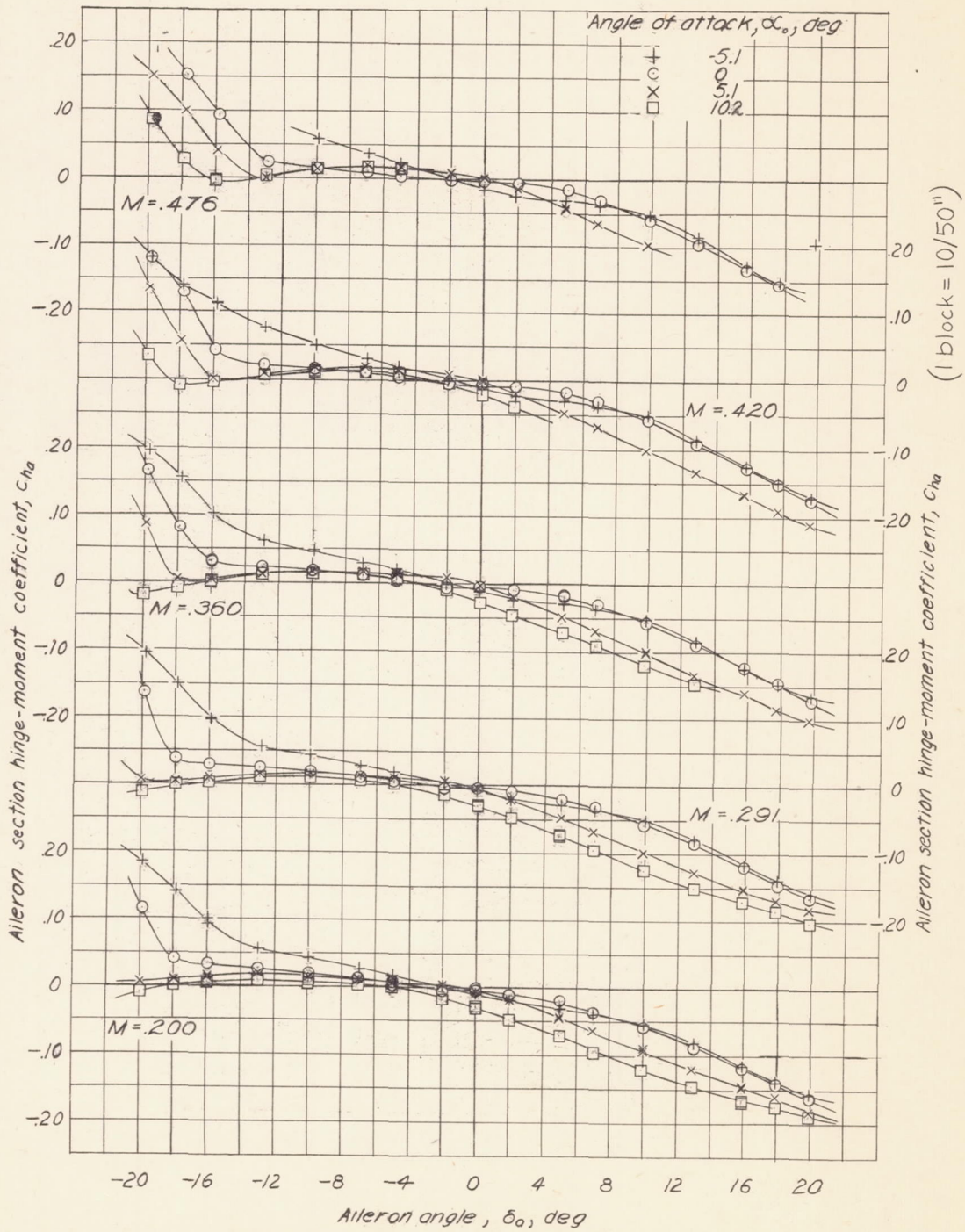

Figure 7. —Variation of aileron section hinge-moment coefficient with aileron angle. Aileron-nose radius = 0.0150c; lower-surface radius = 0; vent gap = 0.0055c.

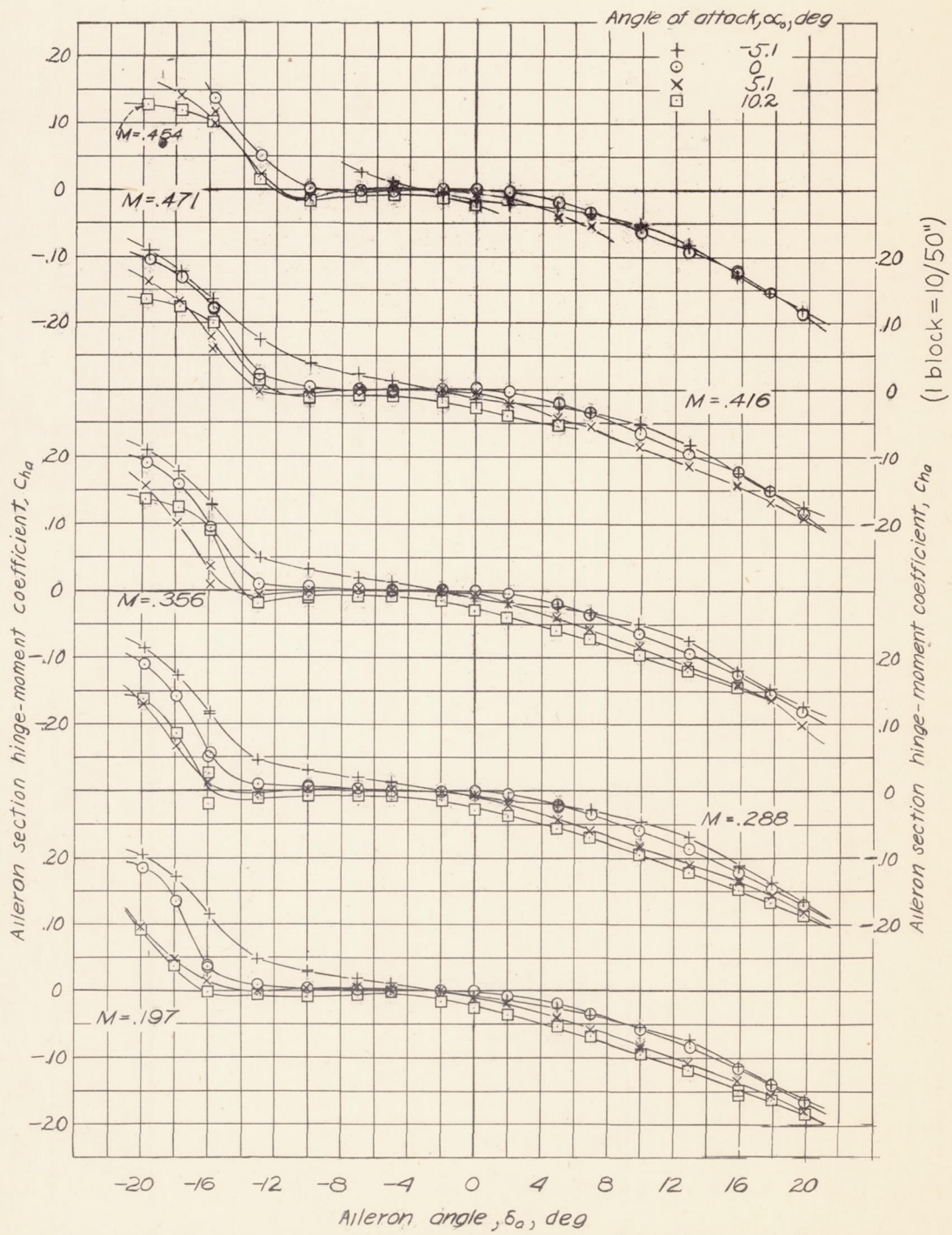

Figure 8. — Variation of aileron section hinge-moment coefficient with aileron angle. Aileron-nose radius = 0.008c; lower-surface radius = 0.02c; vent gap = 0.005c.

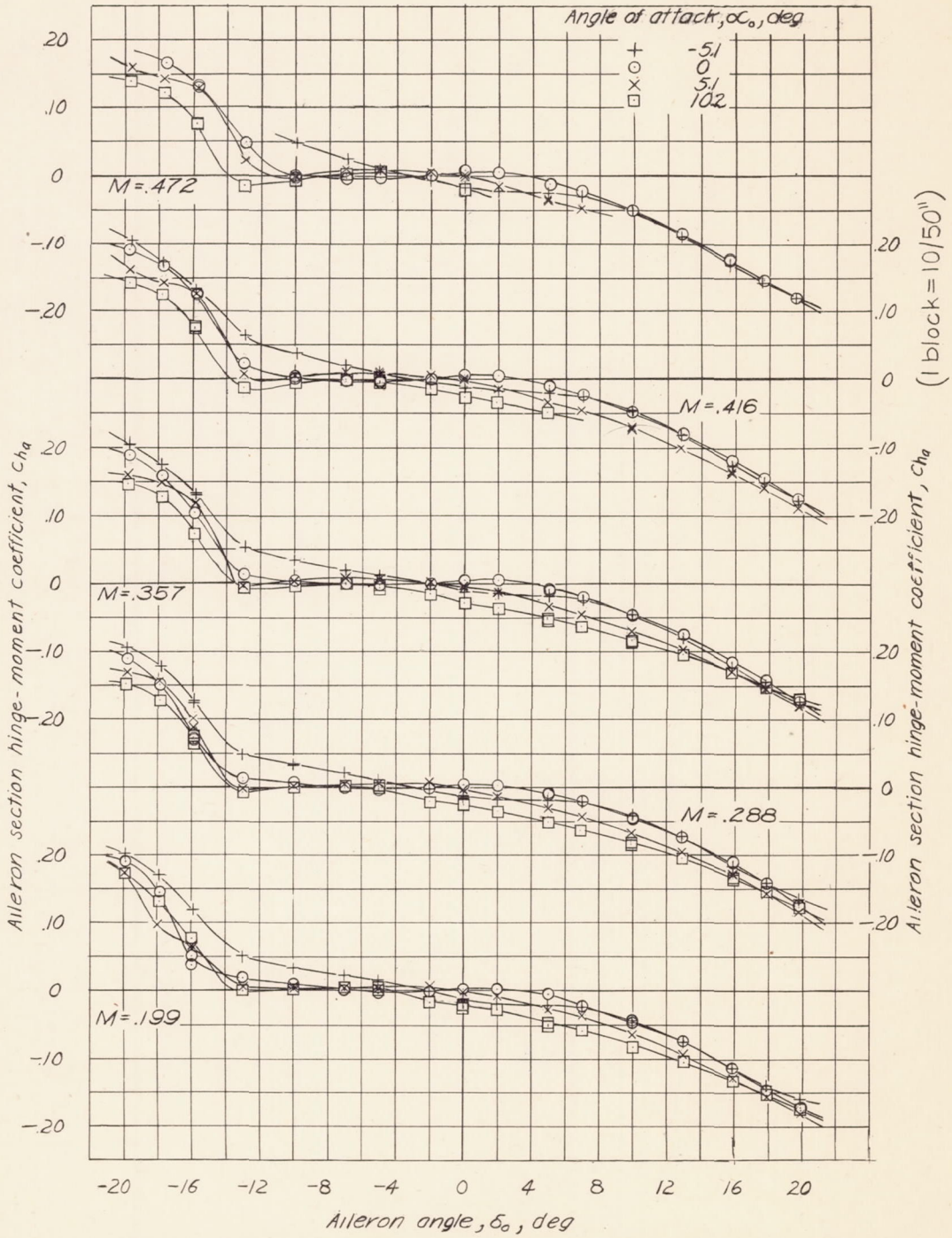

Figure 9. – Variation of aileron section hinge-moment coefficient with aileron angle. Aileron-nose radius = 0.008c; lower-surface radius = 0.02c; vent gap = 0.010c.

(1 block = 10 divisions on 1/32 Arch. scale)

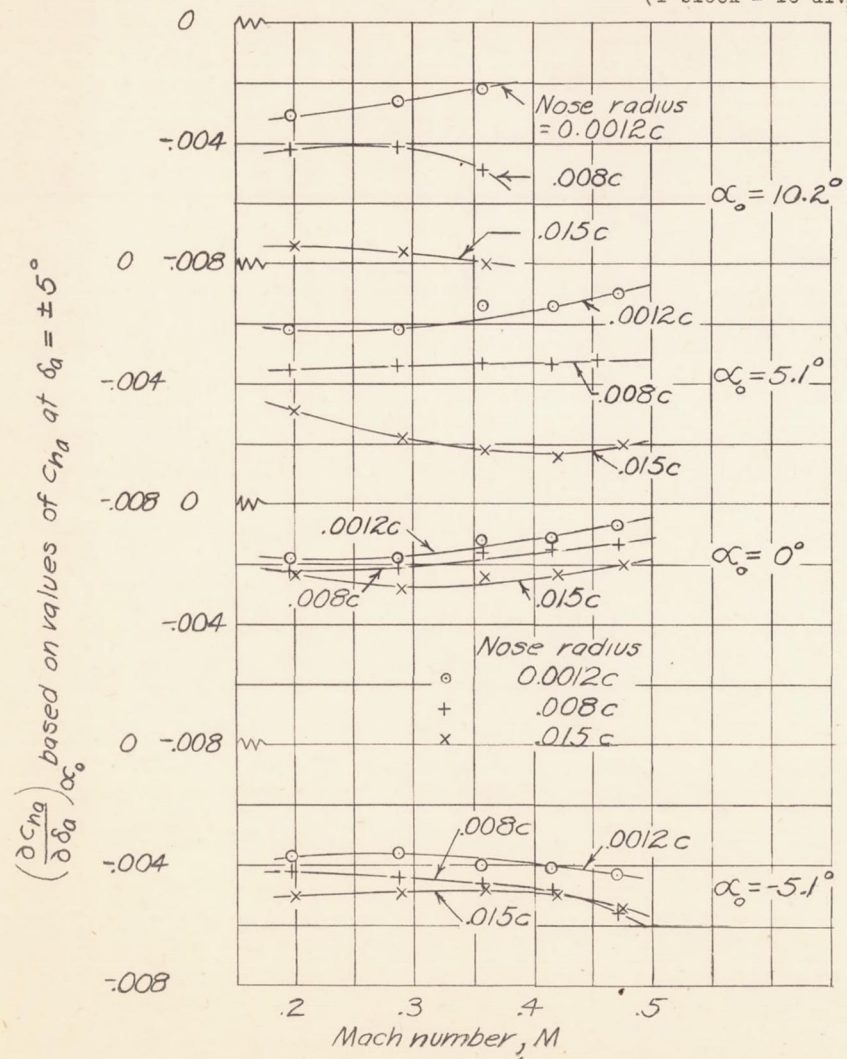

(a) Lower-surface radius = 0; vent gap = 0.0055c.

Figure 10.- Variation of $\left(\frac{\partial C_{n_a}}{\partial \delta_a}\right)_{\alpha_o}$ with Mach number.

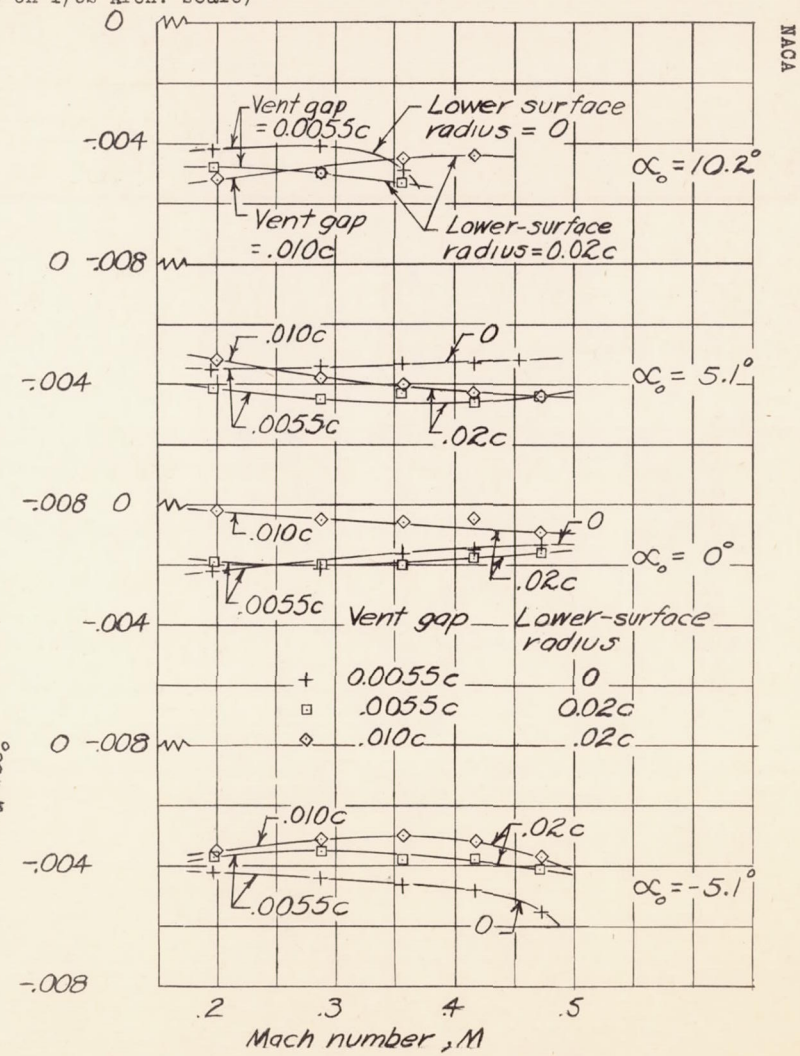

(b) Aileron-nose radius = 0.008c

Figure 10.- Concluded.

NACA

Fig. 10

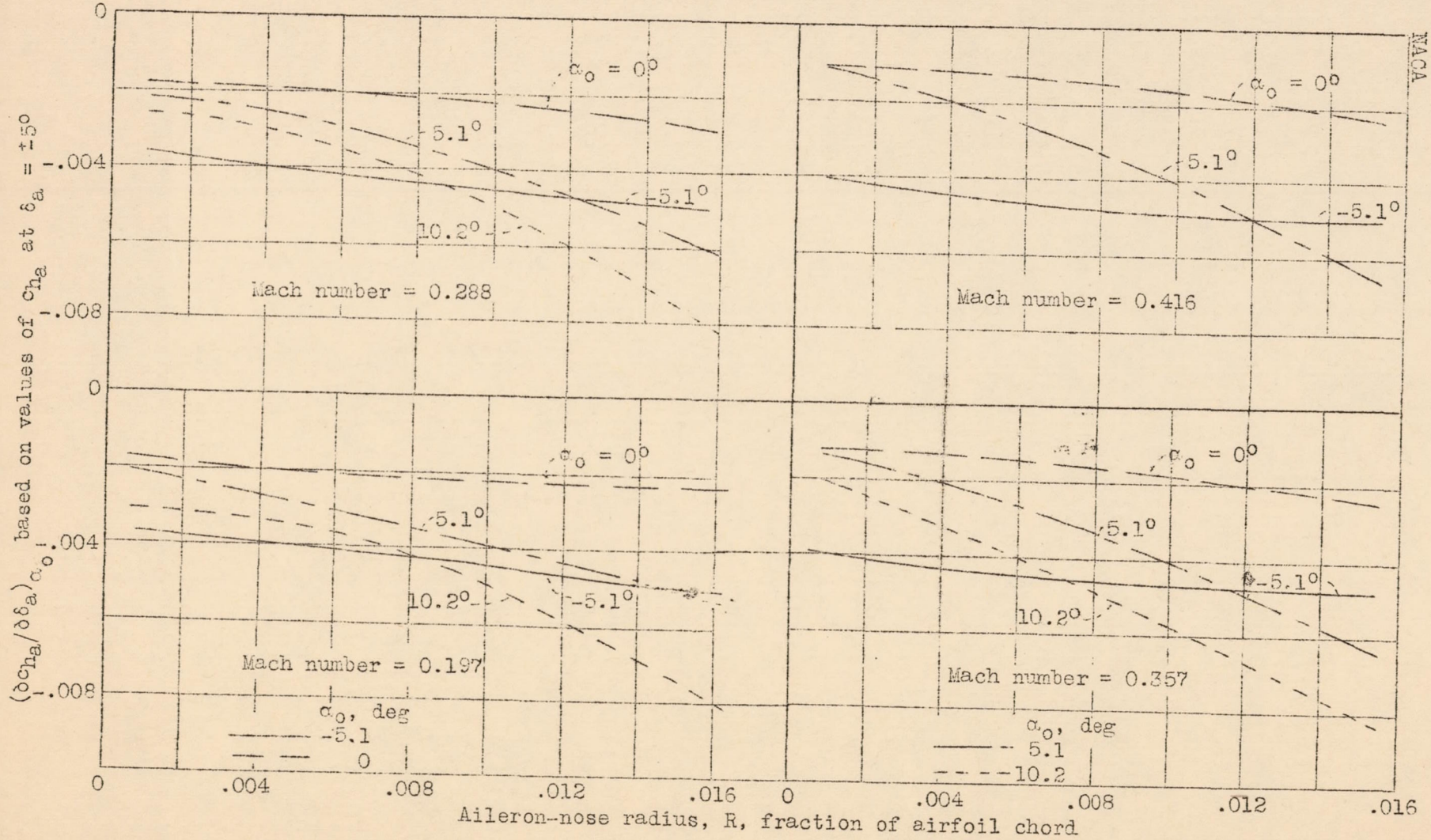

Figure 11.- Variation of $(\partial c_{h_a}/\partial \delta_a)_{\alpha_o}$ with aileron-nose radius. Lower-surface radius = 0; vent gap = 0.0055c.

Fig. 11

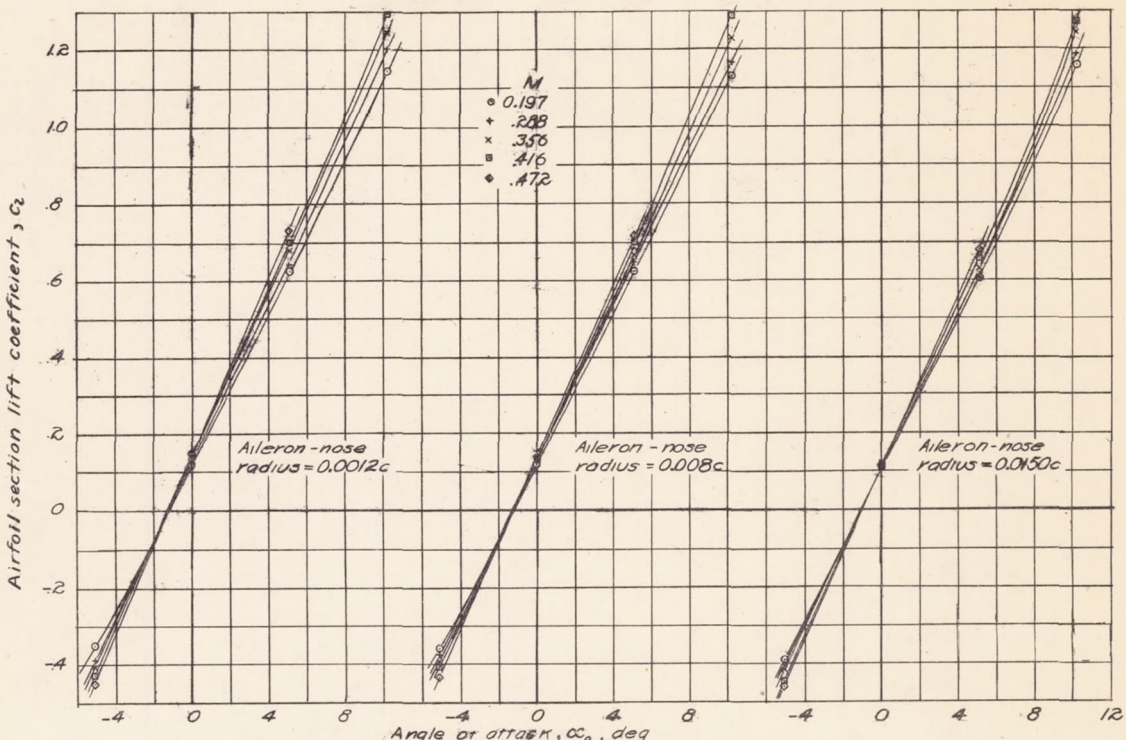

(a) Lower-surface radius = 0; vent gap = 0.0055c.

Figure 12.- Variation of section lift coefficient with angle of attack, $\delta_o = 0$.

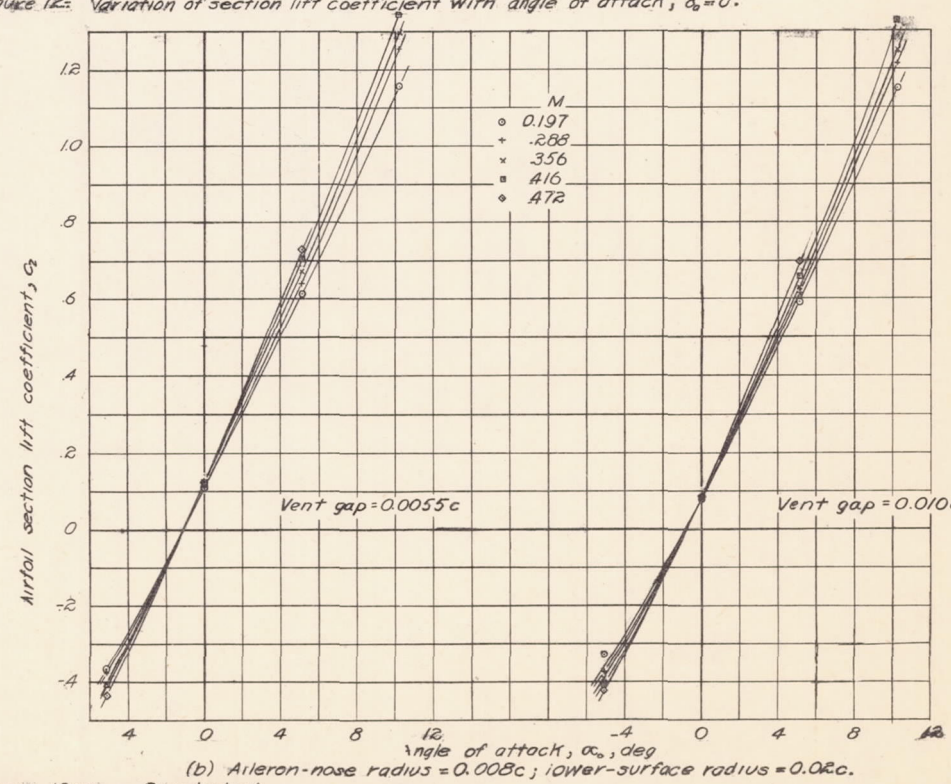

(b) Aileron-nose radius = 0.008c; lower-surface radius = 0.02c.

Figure 12.- Concluded.

(1 block = 10 divisions on 1/50" Engr scale)

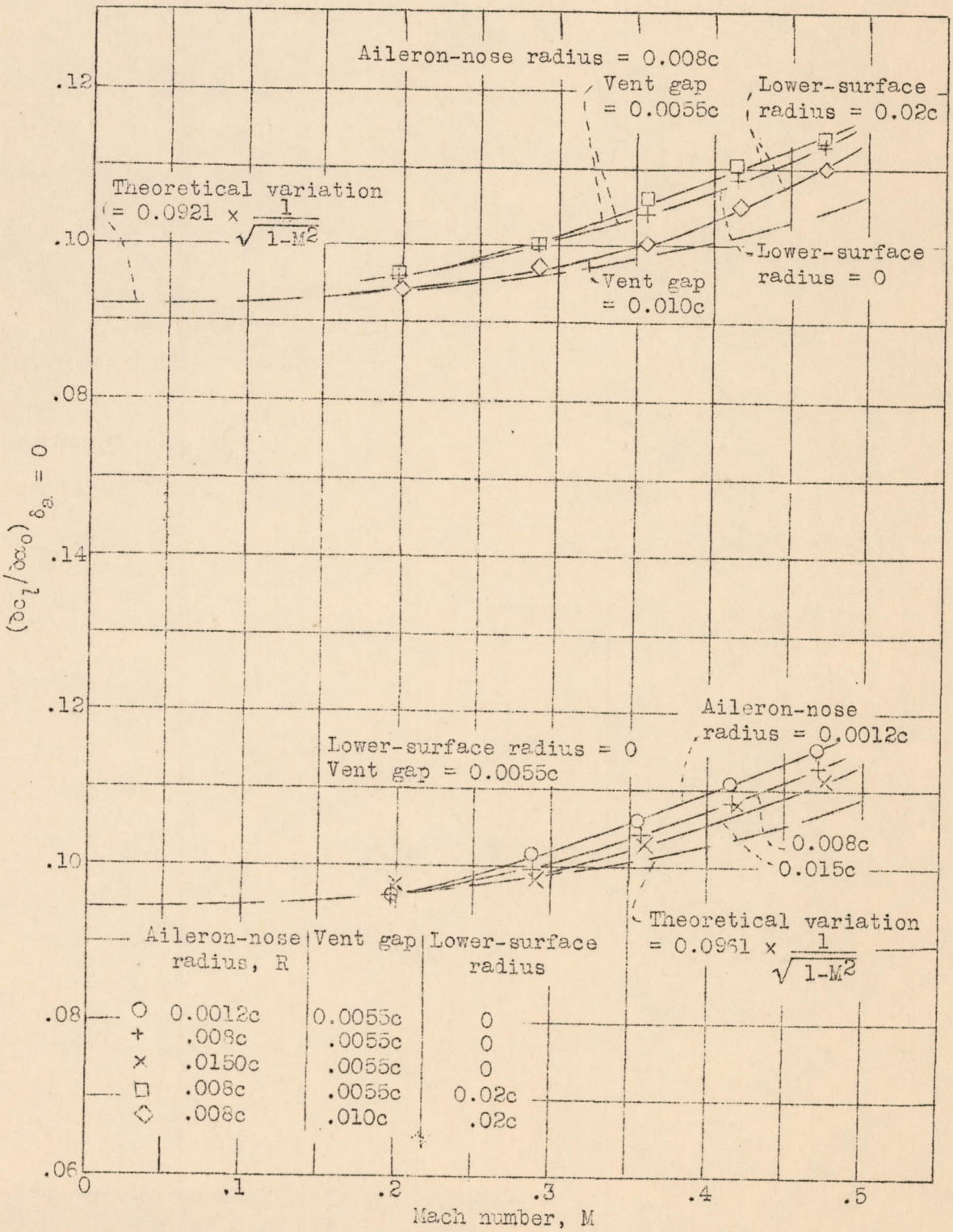

Figure 13.- Variation of lift-curve slope with Mach number, $\delta_a = 0$.

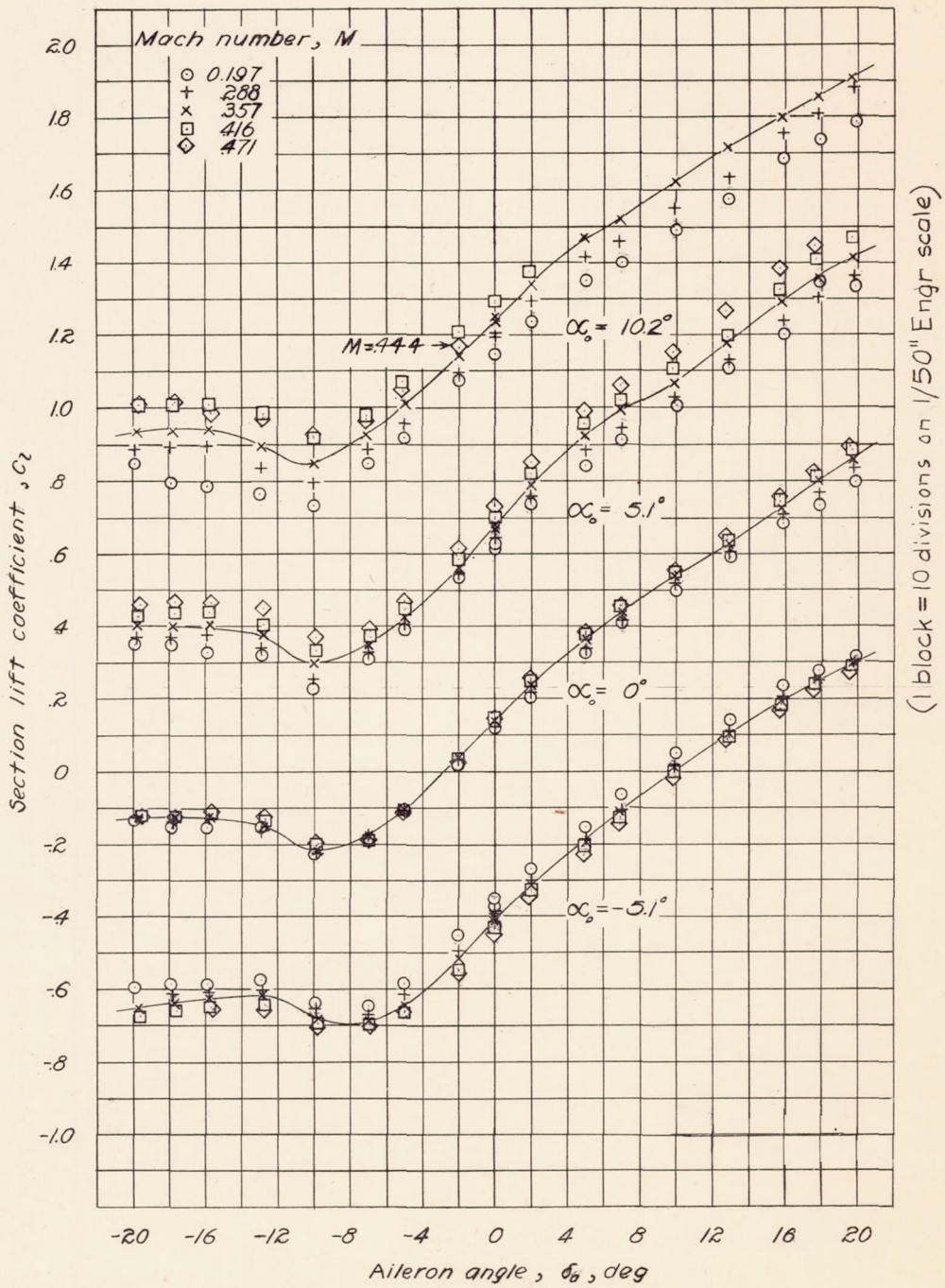

Figure 14.– Variation of section lift coefficient with aileron angle. Aileron-nose radius=0.0012c; lower-surface radius = 0 ; vent gap = 0.0055c.

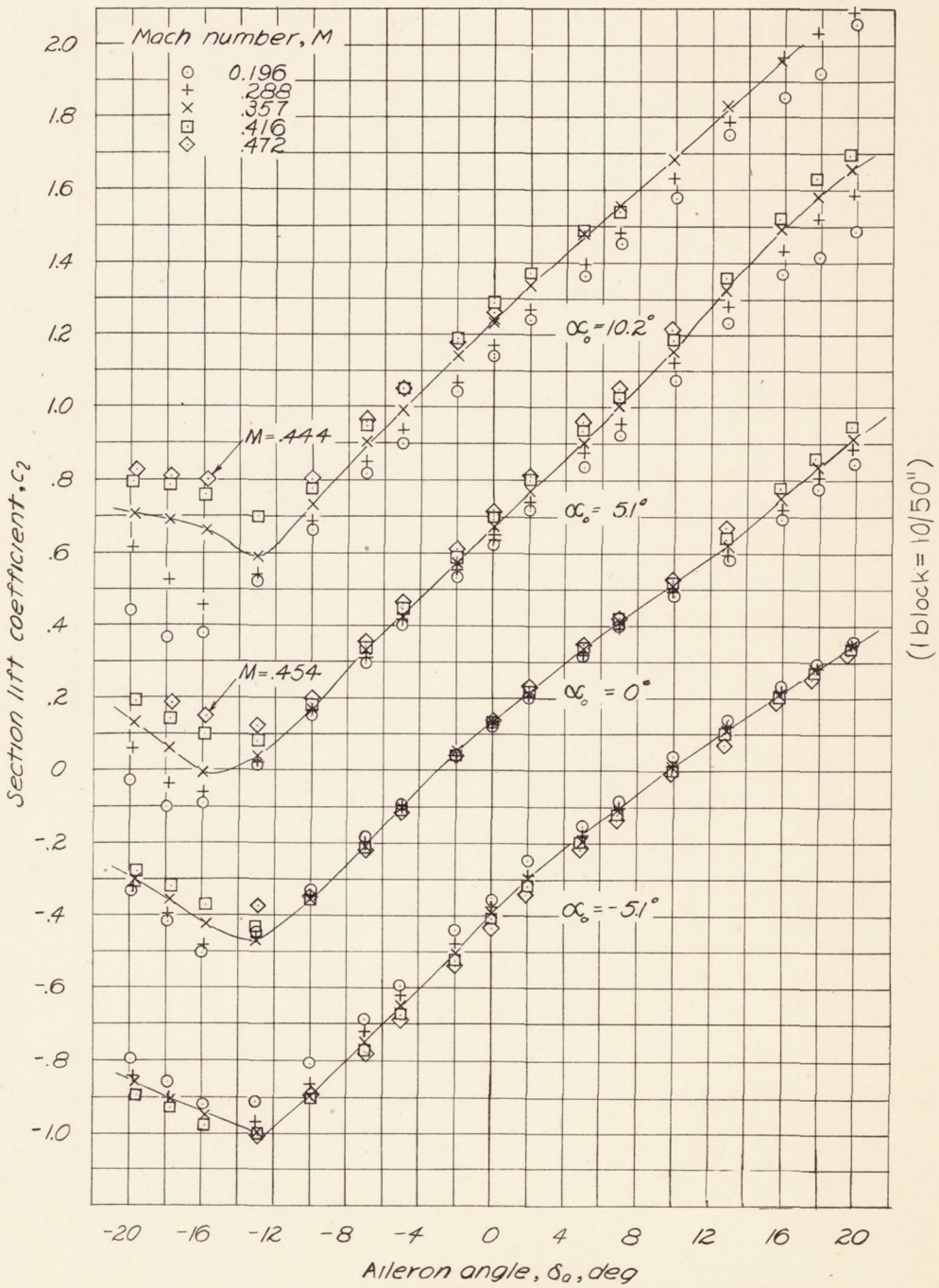

Figure 15. — Variation of section lift coefficient with aileron angle. Aileron-nose radius = 0.008c; lower-surface radius = 0; vent gap = 0.0055c.

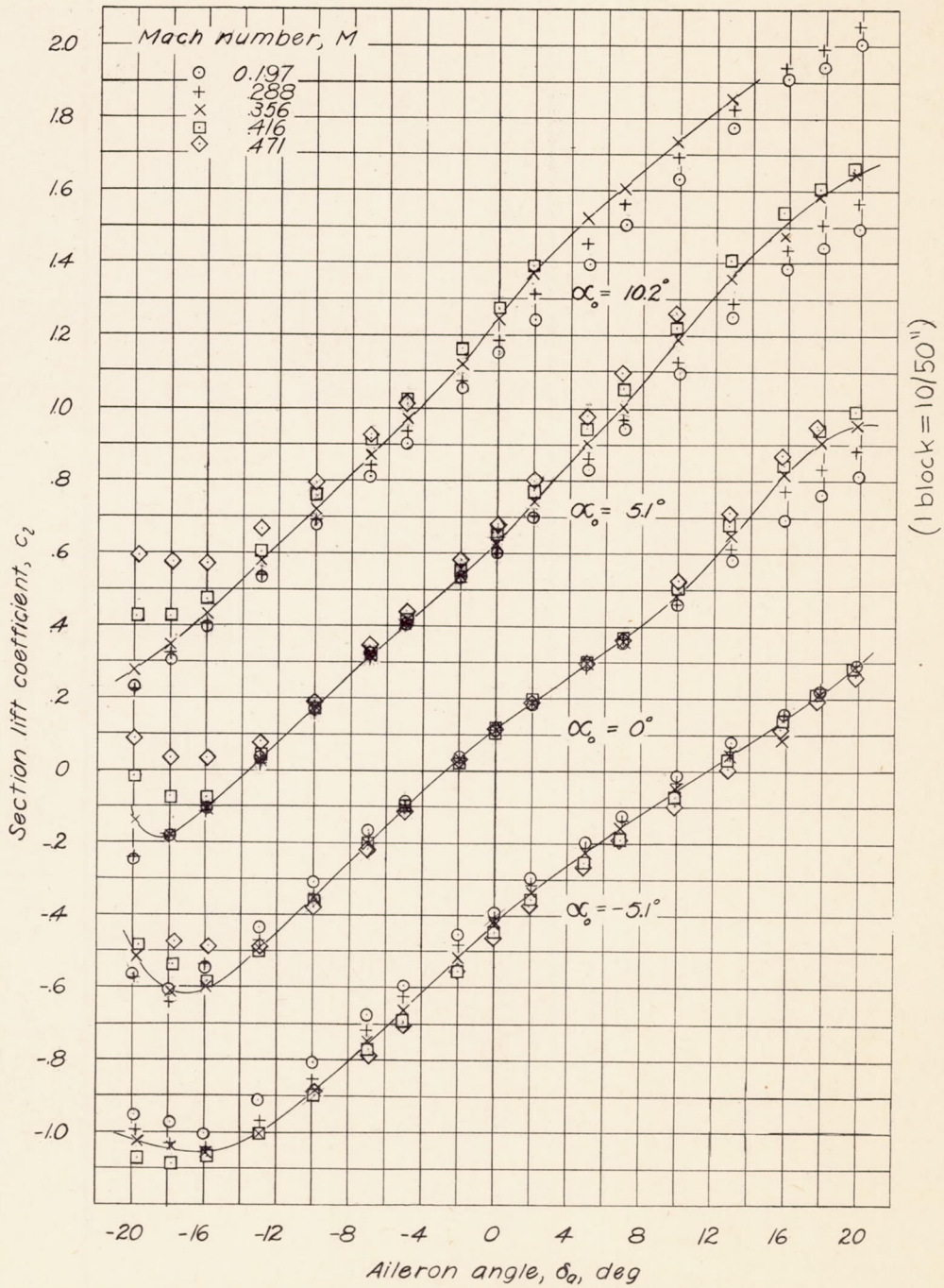

Figure 16.– Variation of section lift coefficient with aileron angle. Aileron-nose radius = 0.0150c; lower-surface radius = 0; vent gap = 0.0055c.

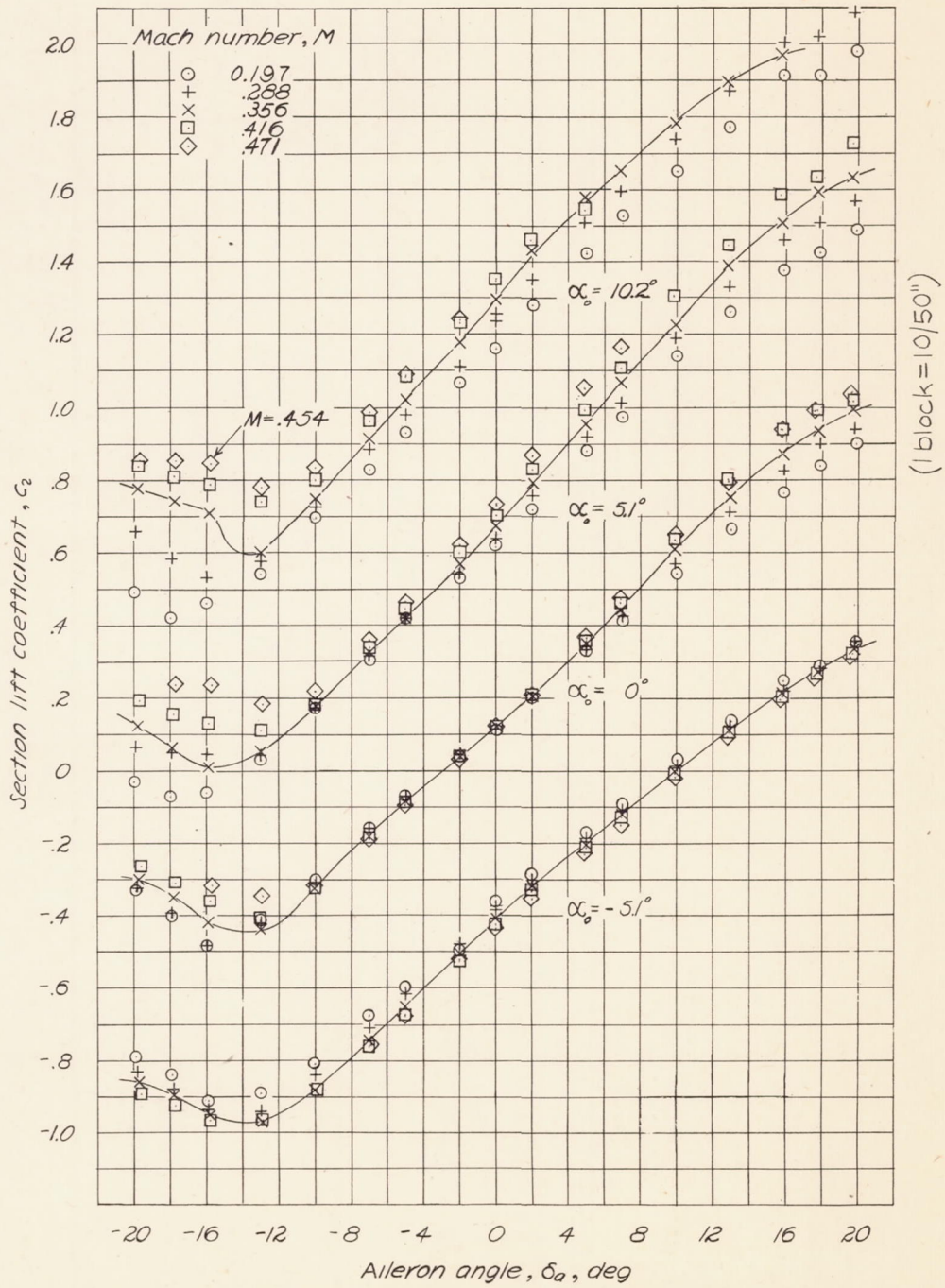

Figure 17.- Variation of section lift coefficient with aileron angle. Aileron-nose radius = 0.008c; lower-surface radius = 0.02c; vent gap = 0.0035c.

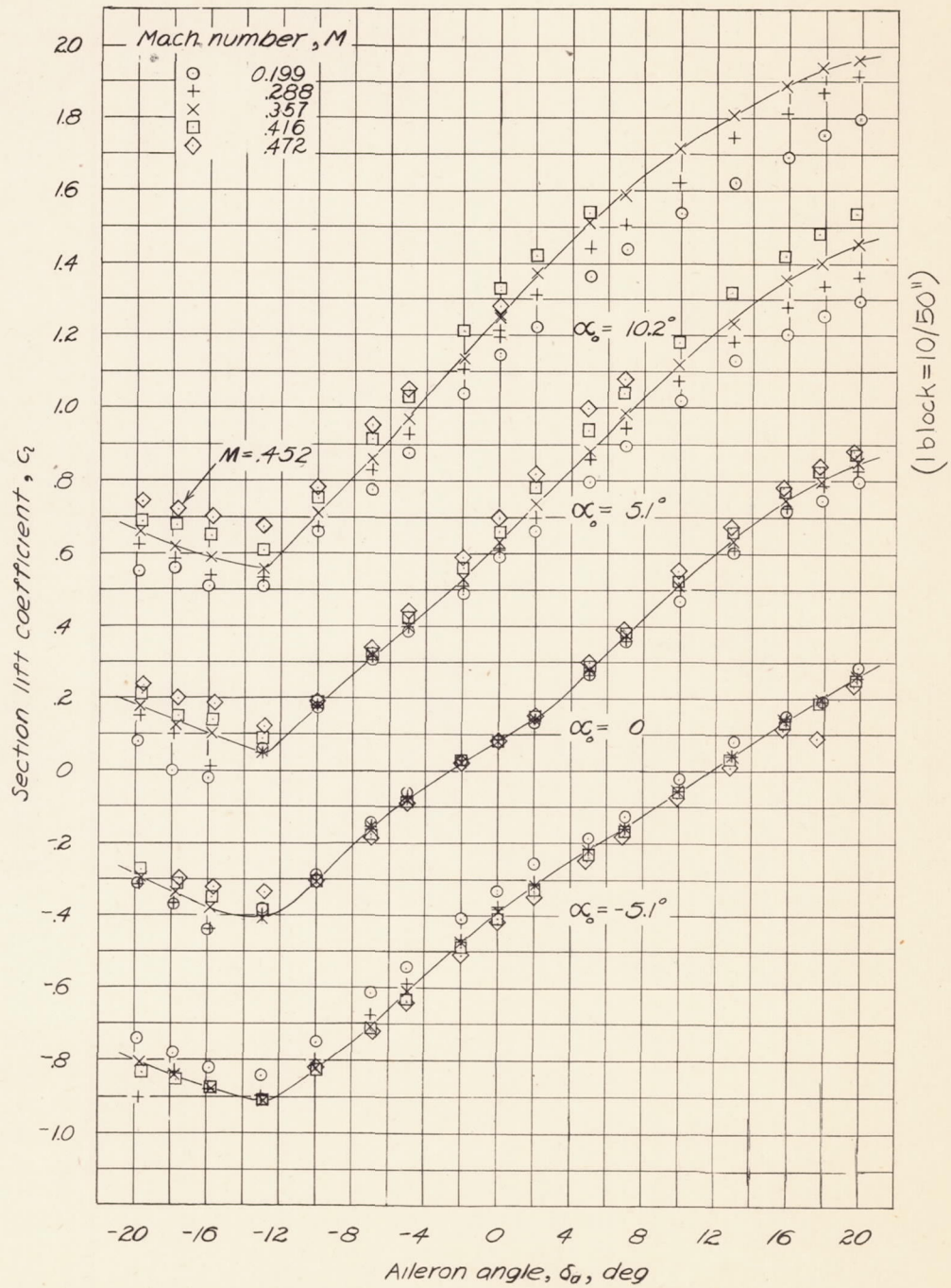

Figure 18. – Variation of section lift coefficient with aileron angle. Aileron-nose radius = 0.008c; lower-surface radius = 0.02c; vent gap = 0.010c.

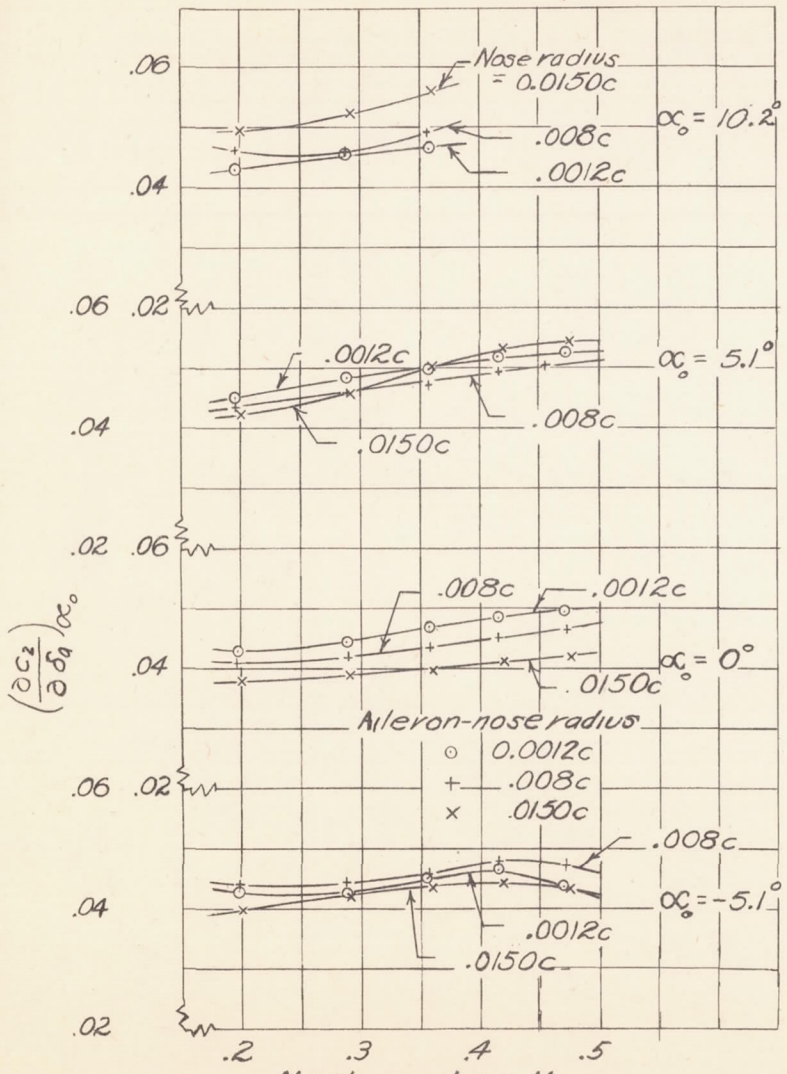

(a) Lower-surface radius = 0; vent gap = 0.0055c.

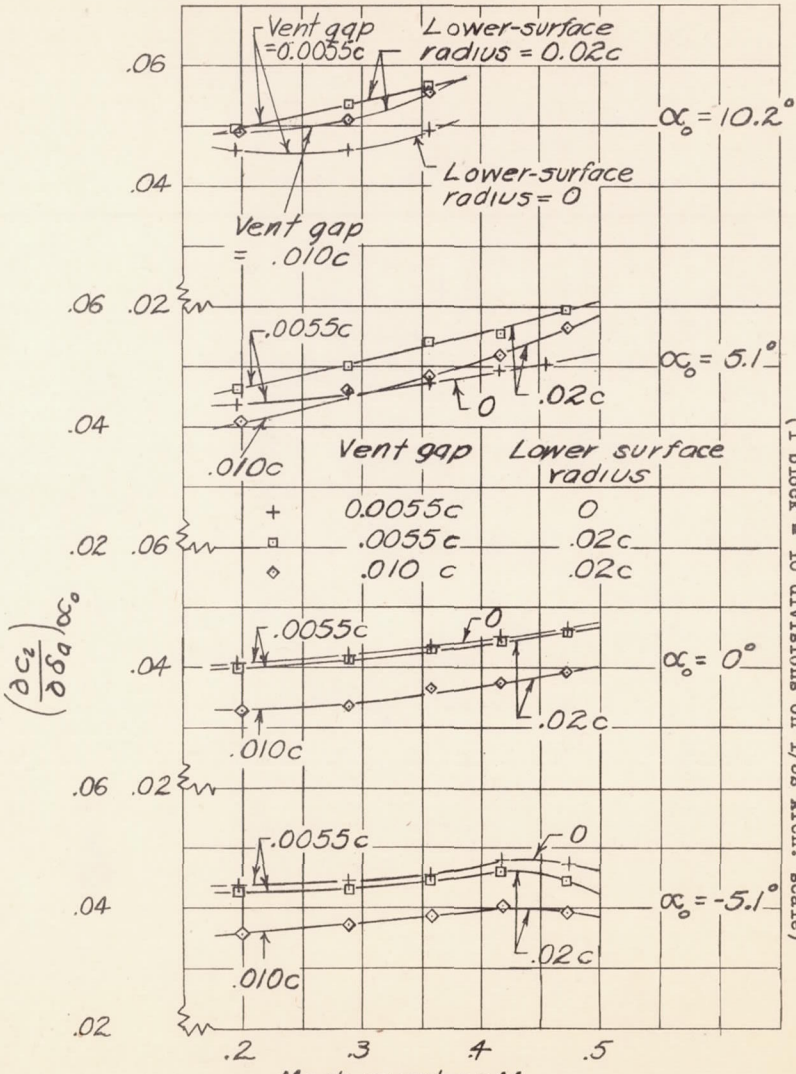

(b) Aileron-nose radius = 0.008c.

Figure 19.- Variation of $\left(\frac{\partial c_z}{\partial \delta_a}\right)_{\alpha_o}$ with Mach number. Figure 19.- Concluded.

(1 block = 10 divisions on 1/32 Arch. scale)

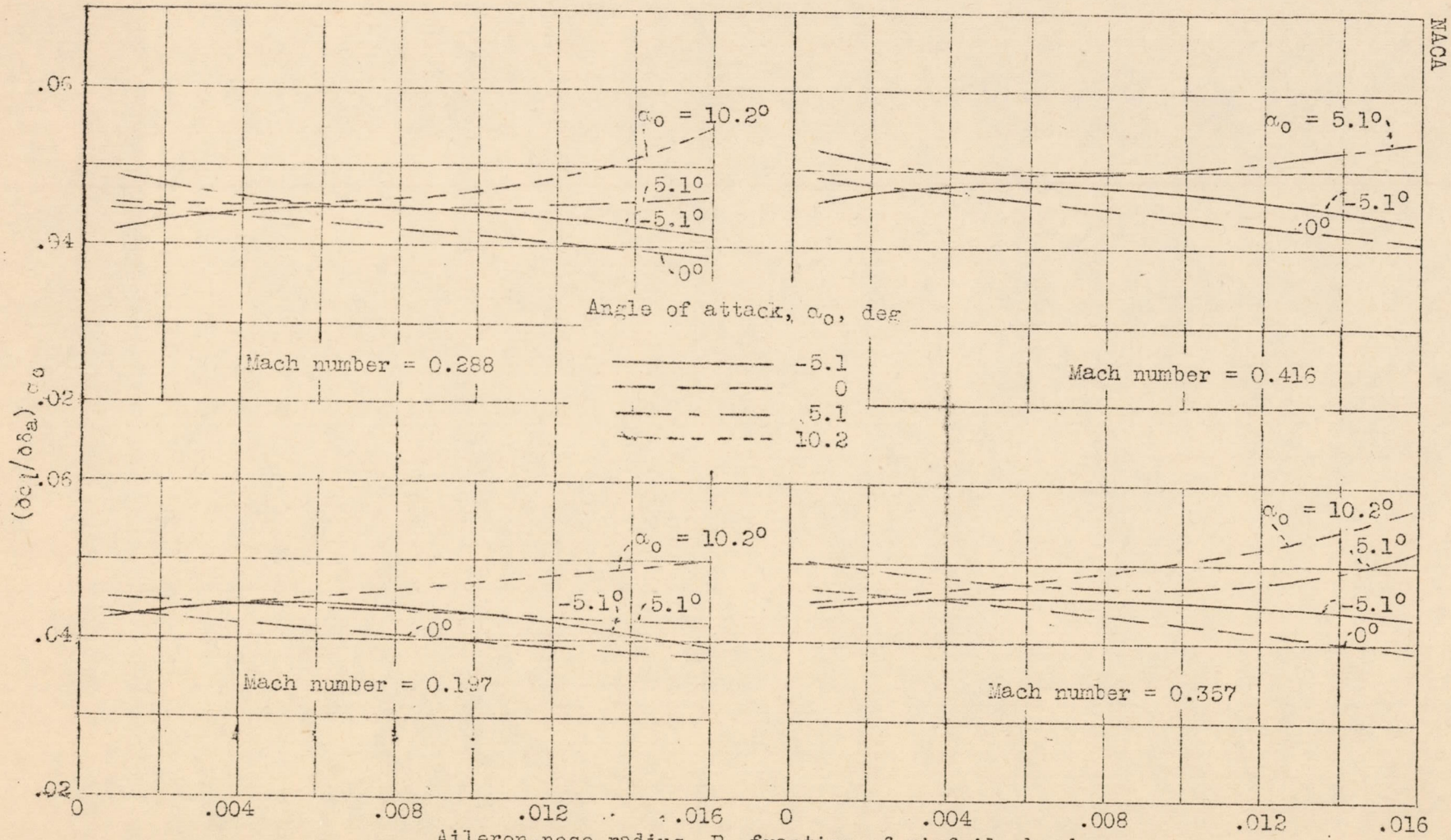

Figure 20.- Variation of $(\partial c_l/\partial \delta_a)_{\alpha_o}$ with aileron nose radius. Lower-surface radius = 0; vent gap = 0.0055c.

Fig. 20